5-1-2012

On the Electronic Spectroscopy of Closed Shell Cations Derived From Resonance Stabilized Radicals: Insights From Theory and Franck-Condon Analysis

T. P. Troy
The University of Sydney

S. H. Kable
The University of Sydney

T. W. Schmidt
The University of Sydney

Scott Reid
Marquette University, scott.reid@marquette.edu

Published version. *Astronomy & Astrophysics,* Vol. 541, No. A8 (May 2012): 1-6. DOI.

A&A 541, A8 (2012)
DOI: 10.1051/0004-6361/201218813

Astronomy & Astrophysics

On the electronic spectroscopy of closed-shell cations derived from resonance-stabilized radicals: Insights from theory and Franck-Condon analysis

T. P. Troy[1], S. H. Kable[1], T. W. Schmidt[1], and S. A. Reid[2]

[1] School of Chemistry, The University of Sydney, NSW 2006, Australia
e-mail: timothy.schmidt@sydney.edu.au
[2] Department of Chemistry, Marquette University, Milwaukee, WI 53233, USA
e-mail: scott.reid@mu.edu

Received 13 January 2012 / Accepted 11 March 2012

ABSTRACT

Context. Recent attention has been directed on closed-shell aromatic cations as potential carriers of the diffuse interstellar bands. The spectra of mass-selected, matrix-isolated benzylium, and tropylium cations were recently reported. The visible spectrum of benzylium exhibits a large Franck-Condon (FC) envelope, inconsistent with diffuse interstellar band carriers.
Aims. We perform a computational analysis of the experimentally studied benzylium spectrum before extending the methods to a range of larger, closed-shell aromatic cations to determine the potential for this class of systems as diffuse interstellar band carriers.
Methods. Density functional theory (DFT), time-dependant ((TD)DFT), and multi-configurational self-consistent field second-order perturbation theory (MRPT2) methods in concert with multidimensional FC analysis is used to model the benzylium spectrum. These methods are extended to larger closed-shell aromatic hydrocarbon cations derived from resonance-stabilized radicals, which are predicted to show strong $S_0 \rightarrow S_n$ transitions in the visible region. The ionization energies of a range of these systems are also calculated by DFT.
Results. The simulated benzylium spectrum was found to yield excellent agreement with the experimental spectrum showing an extended progression in a low frequency (510 cm^{-1}) ring distortion mode. The FC progression was found to be significantly quenched in the larger species: 1-indanylium, 1-naphthylmethylium, and fluorenium. Excitation and ionization energies of the closed-shell cations were found to be consistent with diffuse interstellar band carriers, with the former lying in the visible range and the latter straddling the Lyman limit in the 13−14 eV range.
Conclusions. Large closed-shell polycyclic aromatic hydrocarbon cations remain viable candidate carriers of the diffuse interstellar bands.

Key words. astrochemistry – molecular data – ISM: molecules – ISM: lines and bands

1. Introduction

Light that passes through diffuse material in the interstellar medium is imprinted with absorption bands from hundreds of unidentified species. Collectively known as the diffuse interstellar bands (DIBs), on account of their spectral widths, the identities of their carriers have remained a spectroscopic enigma for nearly 100 years (Sarre 2006; Herbig 1995). While a large body of astronomical work has been undertaken, identifying the carriers is now a problem for laboratory astrophysics. The bands span the visible and near-infrared spectrum, suggestive of molecular electronic transitions. The shapes and spectral widths of the DIBs are consistent with gas-phase molecular carriers. However, the DIBs are largely uncorrelated along different lines of sight, implying unique carriers for each band, and suggesting that carriers must present one absorption band which dominates the spectrum (Hobbs et al. 2009). From the Franck-Condon (FC) principle, this criterion is met when the electronic transition involves a negligible change in nuclear geometry.

Of the molecules known to exist in space, 76% contain carbon, including all species with more than five atoms. Furthermore, studies of the interstellar carbon budget reveal that a large proportion of interstellar carbon is in an unknown chemical form (Snow & Witt 1995). Many candidates have been proposed as carriers of the DIBs, including carbon chains, fullerenes and polycyclic aromatic hydrocarbons (PAHs). Despite decades of study into carbon chains, these have failed to conclusively account for the astronomical features (Maier et al. 2004). Nevertheless, two recent matches between laboratory spectra and DIBs have been reported for the short carbon chains H_2CCC and $HCCCCH^+$; however, these coincidences are still being debated (Linnartz et al. 2010; Maier et al. 2011b; Oka & McCall 2011; Krełowski et al. 2011, 2010). Indeed, after further scrutiny, $HCCCCH^+$ is now regarded as an unlikely carrier of a DIB due to mismatches in the band profile and central wavelength (Maier et al. 2011a). Nevertheless, a large proportion of known interstellar molecules contain the carbon chain motif. Fullerenes were first confirmed as components of circumstellar matter only recently (Cami et al. 2010), and two long wavelength DIBs have been proposed to be due to C_{60}^+ (Foing & Ehrenfreund 1994, 1997) – however, a gas-phase spectrum of that species is still wanting.

Infrared signatures that are highly suggestive of aromatic material can be found in many astrophysical environments,

including star-forming regions and proto-planetary nebulae. These infrared emission bands, variously referred to as the unidentified infrared bands (UIBs) or aromatic infrared bands (AIBs) imply the existence of PAHs in space (Leger & Puget 1984; Allamandola et al. 1985). Of the known gas-phase spectra of neutral, closed-shell PAHs, including up to $C_{42}H_{18}$ (Kokkin et al. 2008), there is no match with a DIB (Salama et al. 2011). Fewer neutral radicals have been studied, but there is an emerging body of work on resonance-stabilized radicals (RSRs) containing up to 13 carbon atoms which suggests that these species are also not DIB carriers (Reilly et al. 2008, 2009; Troy et al. 2009; Sebree et al. 2010; Troy et al. 2011; Chalyavi et al. 2010; Sebree et al. 2011; O'Connor et al. 2011).

Sonnentrucker and co-workers examined the ionization properties of several DIBs, and suggested that the carriers of the 5797 and 6613 Å features should have ionization energies above 10 eV, consistent with singly charged PAHs or fullerenes (Sonnentrucker et al. 1997). PAH cations have received close attention with respect to their candidacy as DIB carriers (Alata et al. 2010; Bréchignac & Pino 1999; Vanderzwet & Allamandola 1985; Leger & D'hendecourt 1985; Allamandola et al. 1985). Salama, Allamandola, and co-workers have systematically examined the spectra of matrix isolated PAH radical cations, generating by in situ VUV photoionization of the isolated PAHs (Salama et al. 1996). Subsequently, Pino and co-workers used resonant two-photon ionization to prepare Ar tagged clusters of PAH cation radicals, which were then photodissociated to yield action spectra that are expected to closely resemble the absorption spectrum of the bare gas-phase cation (Bréchignac & Pino 1999). In the case of the phenanthrene cation radical, the derived oscillator strengh of the $D_0 \rightarrow D_1$ transition (0.15) was some three orders of magnitude larger than inferred from the matrix spectrum. Despite these efforts, no conclusive assignment of a PAH cation radical as a DIB carrier has yet been made. Furthermore, the first absorption for PAH radical cations lies in the infrared, and higher excitations in the visible give rise to very broad features resulting from rapid internal conversion between the close-lying electronic states. While DIBs continue to be found in the infrared region (Geballe et al. 2011), the majority of DIBs are located in the visible region, and open shell cations are not likely carriers of these bands.

A less explored set of molecules are *closed-shell* PAH cations (CSCs). The CSCs present their lowest-lying electronic excitations in the visible region, which should result in spectral line-widths consistent with the DIBs. Many CSCs may be regarded as protonated PAHs, which have recently been the focus of studies by the groups of Jouvet and Maier (Alata et al. 2010; Garkusha et al. 2011b,a), using, respectively, a photodissociation technique and matrix isolation spectroscopy. These tend to show extended vibrational progressions, making them unlikely candidates for the largely uncorrelated DIB features (Hobbs et al. 2009). Another class of CSCs are derived from RSRs, an important class of radicals which are stabilized by resonance. Being less reactive than their non-stabilized counterparts, their concentration can build up to significant levels, and they are important intermediates in a variety of environments including combustion and planetary atmospheres. For example, the 1-phenylpropargyl radical is the dominant aromatic radical observed in the fluorescence spectrum of a benzene discharge (Reilly et al. 2008). These species have low IEs, of the order 6−8 eV, and are thus easily ionized in the ISM. Resonance stabilization is even more important in the cations resulting from ionization of these radicals and, furthermore, the strength of the $S_0 \rightarrow S_1$ transitions in these cations is expected to be larger than the $D_0 \rightarrow D_1$ transitions of the corresponding radicals, requiring a lower column density to bring about a DIB.

Recently, Maier and co-workers reported electronic spectra of mass-selected $C_7H_7^+$ ions (benzylium, tropylium) in a Ne matrix (Nagy et al. 2011a). These CSCs are derived from the well-studied RSRs benzyl and tropyl. The benzylium spectrum appears in the visible region, with the $S_0 \rightarrow S_1$ band origin near 19 300 cm^{-1}, but exhibits a long progression in a low frequency (510 cm^{-1}) ring distortion mode (ν_{13}). This behavior is inconsistent with the carriers of the DIBs. However, this study has raised important questions. Considering benzylium, what changes in structure give rise to the observed progression? Is this progression observed for larger CSCs? What region of the spectrum contains the $S_0 \rightarrow S_1$ transitions of these CSCs? What are the strengths of these transitions? These are some of the questions that we seek to address in the current study, from a theoretical viewpoint.

2. Theoretical procedure

Equilibrium geometries and harmonic ground state frequencies were calculated using the Gaussian 09 (Frisch et al. 2009) and GAMESS (Schmidt et al. 1993) suites of electronic structure programs. Density functional theory (DFT) was used with the M06 functional (Zhao & Truhlar 2008) and Dunning's correlation consistent aug-cc-pVDZ (Dunning Jr. 1989) and aug-cc-pVTZ (Kendall et al. 1992) basis sets. Vertical electronic transition energies and oscillator strengths were calculated for the lowest 15 singlet states using TDDFT with the M06 functional. Subsequently, equilibrium geometries and harmonic frequencies were calculated for selected excited states using the TDM06 functional. Calculations of the $S_0 \rightarrow S_1$ vertical transition energies were also performed with complete active-space self-consistent field (CASSCF) methods combined with a second-order perturbation theory treatment (MRPT2). In these calculations, ROHF orbitals were calculated using optimized DFT, 6-311++G(d,p), geometries. These ROHF orbitals were then used as the starting orbitals for the CASSCF calculations. Excitation energies were obtained at a range of active spaces of N electrons in M orbitals, [N, M] where the maximum N represents the total number of resonant π-electrons for a particular RSR or its CSC. The optimized orbitals obtained at each active space were seeded into the subsequent, larger active space. Reported excitation energies represent values obtained by specifying an equal weighting to both the ground and excited state electronic configurations.

The calculated equilibrium geometries and mass-weighted normal mode displacements from the (TD)DFT calculations were then used as input into a multidimensional FC simulation, using the PGOPHER program suite (Western 2010) which incorporated the full effects of Duschinsky mixing.

Ionization energies were obtained using the B3-LYP functional (Becke 1993; Lee et al. 1988) and the 6-311++G(d,p) basis set.

3. Results and discussion

We begin with the benzylium cation, the $S_0 \rightarrow S_1$ transition of which has recently been observed in a Ne matrix by Maier and co-workers (Nagy et al. 2011a). The (TD)M06/aug-cc-pVDZ calculations predict a vertical excitation wavelength (oscillator strength) for the $S_0 \rightarrow S_1$ transition of 411 nm ($f = 0.026$). The $S_0 \rightarrow S_1$ transition corresponds dominantly to the promotion of

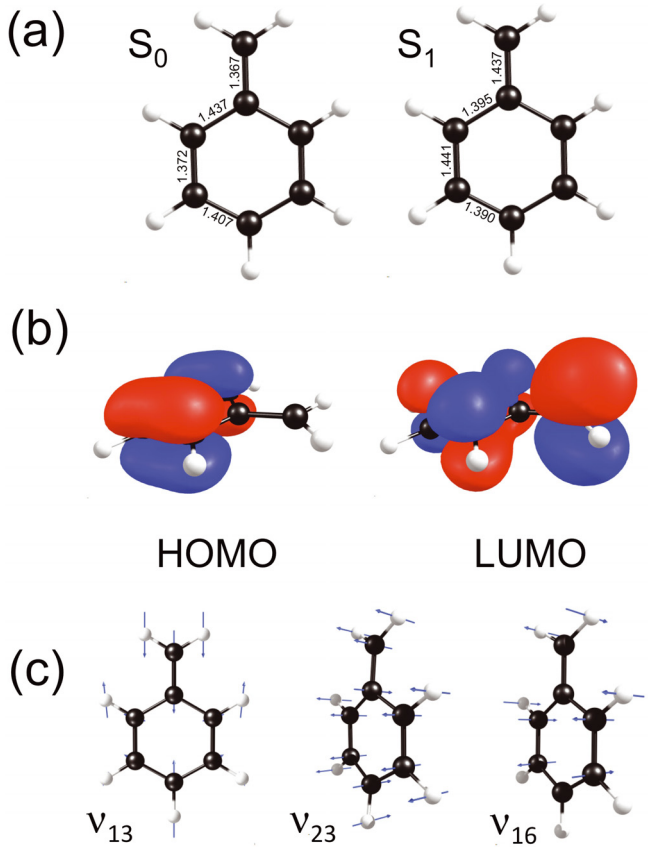

Fig. 1. a) Selected bond lengths of benzylium in the ground and first excited state. **b)** Isosurfaces (0.03 cutoff) of the HOMO and LUMO of benzylium. The $S_0 \rightarrow S_1$ transition corresponds dominantly to the promotion of a single electron from the HOMO to LUMO. **c)** Displacement vectors associated with the FC active modes.

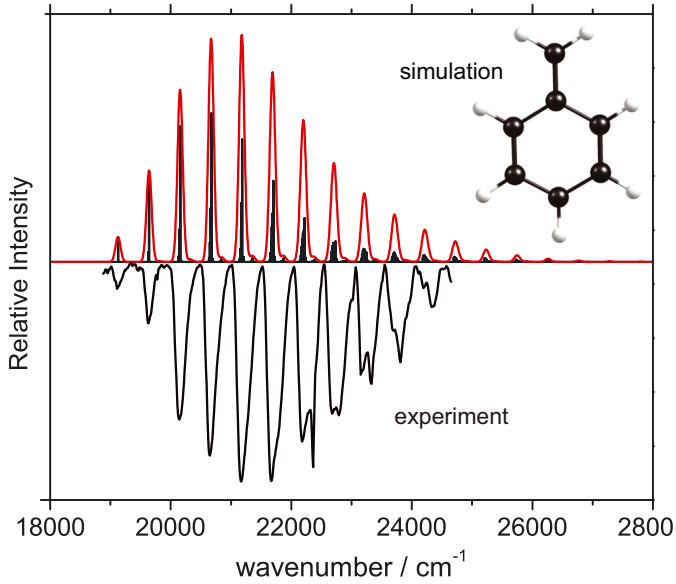

Fig. 2. Calculated FC profile of the $S_0 \rightarrow S_1$ transition of benzylium. The spectrum is shown as a stick spectrum (in black), and convolved with a 100 cm^{-1} FWHM Gaussian profile (red). The experimental spectrum adapted from Nagy et al. (2011a) is shown inverted below.

a single electron from the HOMO to LUMO[1], and isosurfaces (0.03 cutoff) for these orbitals are shown in Fig. 1b. It is evident that a significant geometry change accompanies electronic excitation, with a distortion of the ring along the C_2 axis. We therefore expect FC activity in the totally symmetric in-plane ring distortion, and Fig. 1c. shows the displacement vectors associated with this mode (ν_{13} in the Mulliken notation). The calculated frequency of this mode (515 cm^{-1}) in the S_1 state closely matches the frequency reported by Maier and co-workers in their Ne matrix spectrum (510 cm^{-1}). In addition, we find two non-totally symmetric modes that undergo significant frequency changes in the electronic transition. These are associated with out of plane ring and methylene distortions, and the displacement vectors for these modes (ν_{23}, b_1; ν_{16}, a_2) are also shown in Fig. 1c. The results from these calculations, including the geometries, harmonic frequencies, and mass-weighted normal mode displacements, were then used as input into a FC simulation that incorporated the effects of Duschinsky mixing and included the three modes described above (ν_{13}, ν_{16}, ν_{23}). In other simulations, we included additional a_1 modes, but these displayed weak activity. The calculated spectrum is shown in Fig. 2, as both a stick spectrum and convolved with a Gaussian profile of 100 cm^{-1} full width at half maximum in order to more closely mimic the observed matrix spectrum. The position of the origin band has been set at the value observed by Maier and co-workers in the Ne matrix. A long progression in ν_{13} is observed, the breadth of which is similar to the experimental spectrum of Maier and co-workers. As expected, activity is also observed in the non-totally symmetric modes (ν_{16}, ν_{23}). Our simulation suggests that the broad linewidths observed in the experimental spectrum most likely reflect inhomogenous broadening from the matrix environment. It is worth noting here that the $D_0 \rightarrow D_1$ spectrum of phenanthracene cation radical in the gas-phase exhibits much sharper structure than found in the Ne matrix (Bréchignac & Pino 1999). We have performed additional calculations using MRPT2 methods to predict the vertical transition energies of the $S_0 \rightarrow S_1$ spectrum of benzylium and a selection of related CSCs containing fewer than 12 carbon atoms, for which neutral radical spectra have been recorded in the gas-phase. The results of these calculations are compared with the limited available experimental data in Fig. 3, where the labels refer to the corresponding RSR. The calculated vertical excitation energy of benzylium is in good agreement with the peak of the FC progression in the experimental spectrum (Nagy et al. 2011a). Notable in this figure is the behavior of the $S_0 \rightarrow S_1$ transition energy, which for all but the smallest cations lies in the visible spectrum. The calculated (TDDFT) oscillator strengths of the $S_0 \rightarrow S_1$ transitions for these cations are sizeable: benzylium, $f = 0.026$; indanylium, $f = 0.043$; 1-naphthylmethylium, $f = 0.059$. The strength of the $S_0 \rightarrow S_1$ transitions in these cations are larger than the $D_0 \rightarrow D_1$ transitions of the corresponding radicals ($O(10^{-3})$); this is due to the fact that, in the radicals, the $D_0 \rightarrow D_1$ transitions reflect single electron excitations from SOMO $\rightarrow$ LUMO and HOMO $\rightarrow$ SOMO, and these transition moments cancel to an extent.

Additional FC simulations were performed for selected closed-shell cations, in order to examine the evolution in the spectrum with increasing number of rings. Figure 4a displays the optimized structures and isosurfaces (cutoff = 0.03) of the HOMO and LUMO for indanylium, derived from the indanyl radical, the electronic spectroscopy of which has been experimentally characterized by our group (Troy et al. 2009). Figure 4b displays corresponding information for 1-naphthylmethylium, derived from the 1-naphthylmethyl radical. In comparison with benzylium, the bi-cyclic systems show more extended

[1] HOMO – highest occupied molecular orbital, LUMO – lowest unoccupied molecular orbital.

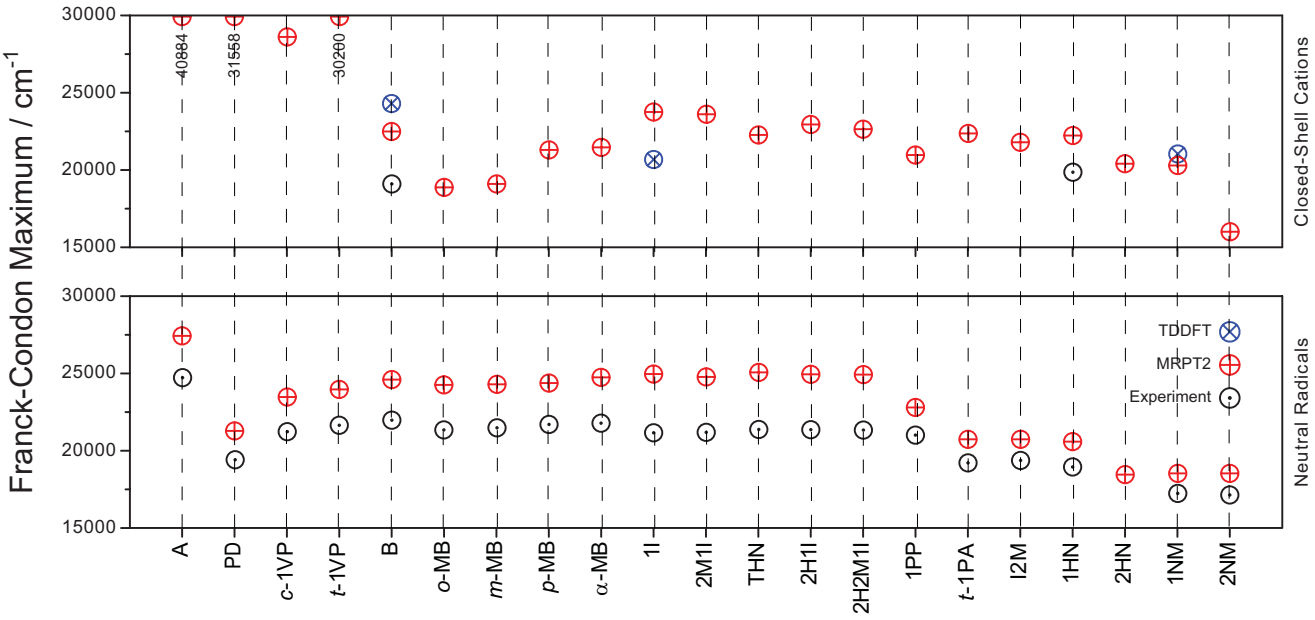

Fig. 3. *Top*: calculated vertical transition energies of the $S_0 \rightarrow S_1$ transition of a variety of closed-shell cations(CSCs) derived from resonance stabilized radicals (RSRs), arranged in increasing chromophore size. *Bottom*: calculated vertical transition energies of the $D_0 \rightarrow D_1$ transition of a variety of resonance stabilized radicals. *Key*: A – allyl; PD – pentadienyl; c-1VP – *cis*-1-vinylpropargyl; t-1VP – *trans*-1-vinylpropargyl; B – benzyl; o-MB – *ortho*-methylbenzyl; m-MB – *meta*-methylbenzyl; p-MB – *para*-methylbenzyl; 1I – 1-indanyl; 2MI1 – 2-methylindan-1-yl; THN – 1,2,3-trihydronaphthyl; 2HI1 – 2-hydroxyindan-1-yl; 2H2MI1 – 2-hydroxy-2-methylindan-1-yl; 1PP – 1phenylpropargyl; t-1PA – *trans*-1-phenylallyl; I2M – indan-2-ylmethyl; 1HN – 1-hydronaphthyl; 2HN – 2-hydronaphthyl; 1NM – 1 naphthylmethyl; 2NM – 2-naphthylmethyl.

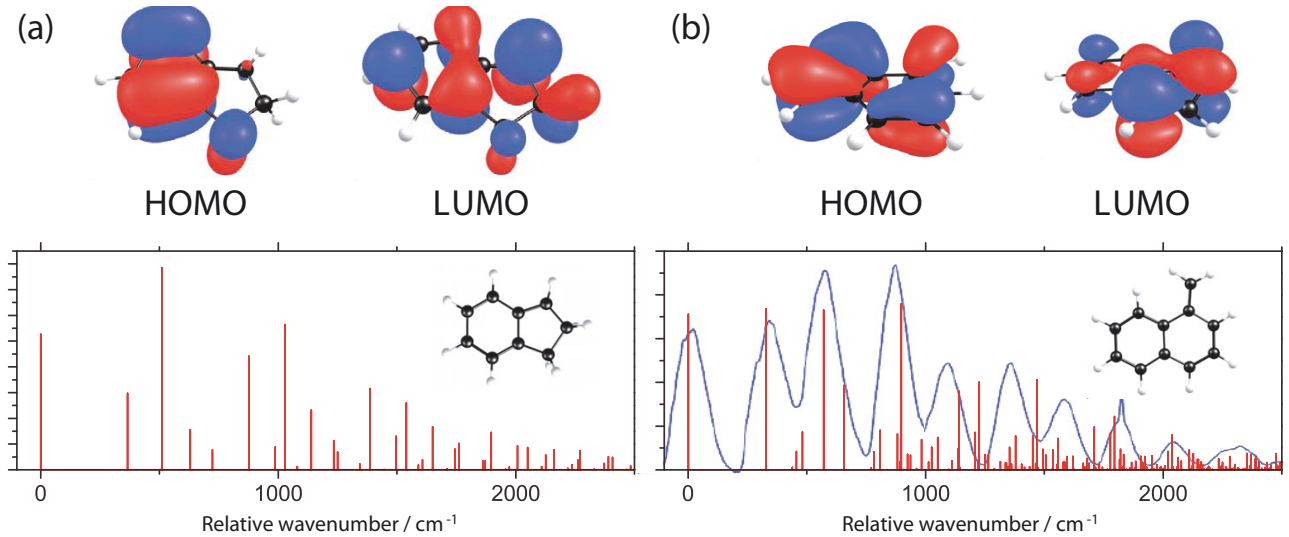

Fig. 4. a) Simulated FC profile of the $S_0 \rightarrow S_1$ transitions of indanylium; and illustrations of its calculated equilibrium structure and HOMO and LUMO isosurfaces (0.03 cutoff). **b)** Same as **a)**, but for 1-naphthylmethylium. The experimental spectrum was taken from Nagy et al. (2011b).

delocalization of both HOMO and LUMO, as expected. Figure 4 also shows the simulated FC profiles for these two cations, generated using the protocol described above. The simulations included the lowest frequency totally symmetric modes, in addition to any active non-totally symmetric modes. Considering the indanylium cation, activity in the benzene-like ring-distortion mode is seen, but is significantly quenched in comparison with benzylium. In contrast, the simulated 1-naphthylmethylium spectrum shows no extended progressions in any single mode. Therefore, the pronounced vibronic structure observed for benzylium is quenched in these CSCs. The experimental spectrum of Nagy et al., which was published during the preparation of this contribution, confirms of our predicted naphthylmethylium spectrum (Nagy et al. 2011b).

Extending this to tri-cyclic systems, we performed a similar analysis on the fluorenylium cation ($C_{13}H_9^+$), noting that Jouvet and co-workers have recently measured the spectrum of protonated fluorene ($C_{13}H_{11}^+$) (Alata et al. 2012). TDDFT calculations at the TDM06/cc-pVDZ level show transition energies and oscillator strengths for the $S_0 \rightarrow S_1$ and $S_0 \rightarrow S_2$ transitions of 883 nm ($f = 0.002$) and 439 nm ($f = 0.24$). The $S_0 \rightarrow S_1$ transition again corresponds to a one-electron excitation from HOMO to LUMO, shown in the upper panel of Fig. 5. The calculated FC profile for the $S_0 \rightarrow S_1$ transition is shown in Fig. 5a,

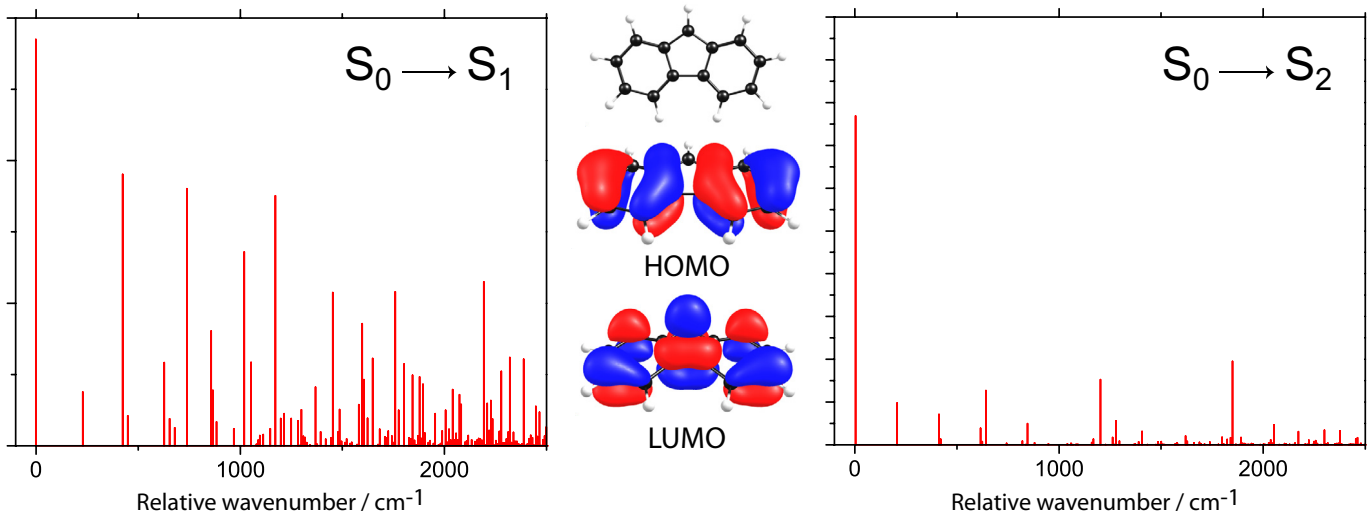

Fig. 5. *Left*: calculated FC profile of the $S_0 \rightarrow S_1$ transition of fluorenium. *Right*: calculated FC profile of the $S_0 \rightarrow S_2$ transition of fluorenium. *Center*: illustrations of the calculated equilibrium structure of fluorenium, and its HOMO and LUMO isosurfaces (0.03 cutoff).

where the lowest eleven a_1 modes were included. It is clear that, compared with the other systems, less extensive FC activity is observed, and the origin feature gains in intensity compared to higher energy features. This, of course, is partially due to the higher symmetry of this species (i.e., C_{2v} vs. C_s). As the very strong $S_0 \rightarrow S_2$ transition is also predicted to lie in the visible region, we carried out a FC similation of this band, which is shown in Fig. 5b. The TDDFT calculations show that this transition largely reflects a one-electron excitation from HOMO-1 to LUMO, which induces a small geometry change in the excited state. As a result, the calculated FC profile is dominated by the large origin feature.

To further assess the viability of these cations as DIB carriers, we examined their ionization energies. The first ionization energies were calculated for a range of radicals, with the calculated vertical and adiabatic ionization energies consistently within 0.1 eV of experiment using the B3-LYP/6-311++G(d,p) procedure. Interestingly, it was found that the chemically accurate G3X(MP2)-RAD method consistently overestimated the IE as compared to experiment by about 0.07 eV, while the less expensive density functional method underestimates by about 0.08 eV (Troy et al. 2011). There is less experimental data available for the second IE, which connects the cation to the dication. The results of these calculations are shown in Fig. 6. The energy required to remove an electron from the singly ionized species broadly decreases with increasing ion size, as expected. For the species containing nine carbon atoms or more, the second IE is in the range 13−14 eV. The calculations are generally on the lower side of the experimental range; however, we can compare to a study by Rabrenovíc and coworkers, who used a charge-stripping technique to measure the IEs of hydrocarbon cations with the formula C_xH_y where $x = 1$−9, and $y = 0$−8, produced from over 30 hydrocarbon precursors (Rabrenovíc et al. 1983). The reported values represent the IE recorded for a particular $[C_xH_y]^+$ mass channel averaged over several experiments and at least three different hydrocarbon precursors. The values may therefore represent the average of several isomeric forms and as such the carrier of a particular mass channel is by no means certain. Nevertheless, if we assume, for example, that C_3H_5 is carried by the allyl radical, and that C_9H_7 is carried by the 1-phenylpropargyl radical then some comparisons may be made

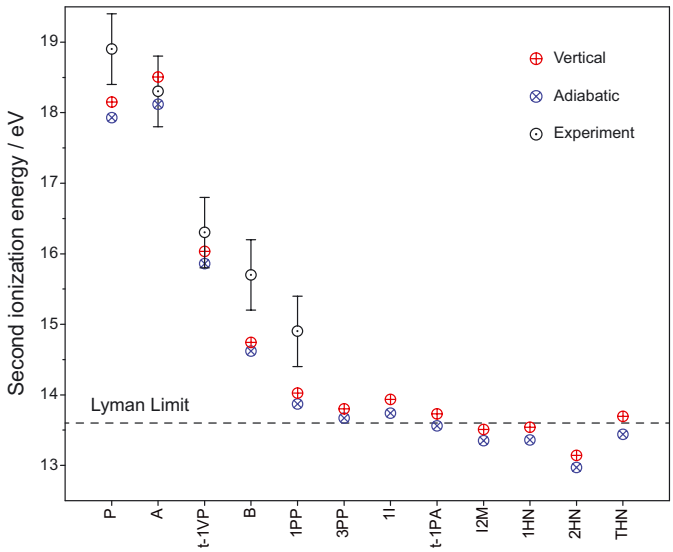

Fig. 6. Comparison of the calculated B3-LYP/6-311++G(d,p) vertical and adiabatic second IEs with experimental values (Rabrenovíc et al. 1983). See Fig. 4 for molecular labels. P – propargyl(ium).

despite the uncertainty in the carrier assignment. The authors report that several compounding factors can lead to errors as high as ±0.5 eV. Despite their discussion of the source of these potential errors, no error values are specified. As such, the largest error is here assumed. The calculated vertical second IEs are found to have a mean absolute difference (MAD) between calculation and experiment of 0.61 eV, which is significantly higher than the MAD of 0.08 eV that was found for the first IEs. However, considering the uncertainty in the chemical assignment of the mass carriers, and the high error in the reported values, this comparison at least demonstrates that the present calculated IEs are in the appropriate range for these cations. As shown in Fig. 6, the calculated cation IEs show the same propensity as the calculated neutral IEs for underestimating the experimental values and the same downward trend with increasing system size.

In the work of Malloci and co-workers (Malloci et al. 2007), calculations include the IEs of the open-shell cations

of 40 closed-shell PAHs. For six of their systems there exists experimental data measured by both charge-stripping and electron-impact techniques and as such these experimental results are likely more reliable. Their data shows a MAD from experiment of 2.29 and 2.23 eV for the adiabatic and vertical values, respectively. This compares with a MAD of 0.74 and 0.61 eV in the present work.

Doubly ionized species are subject to dissociation by coulombic forces. As such, it is accepted that second ionization will lead to destruction of a molecule in the diffuse medium (Allain et al. 1996). That the calculated second ionization energies are in the 13−14 eV range is of interest: this range of IEs straddles the Lyman limit at 13.6 eV. Jenniskens et al. studied the environmental behavior of DIB strengths, showing that both the first and second IE of the λ6196 carrier are at lower photon energies than the λ6284 carrier (Jenniskens et al. 1994). From the strength of the λ6284 DIB at low reddening, it is concluded that its carrier is resilient to photons of energy <13.6 eV. That the λ6196 carrier is depleted in the Orion nebula suggests destruction at photon energies <13.6 eV. As such, there is observational evidence for the second IE of DIB carriers straddling the 13.6 eV threshold, as calculated for the CSCs considered here. In a later study, Sonnentrucker et al. conclude that the λ5780, 5797 and 6613 DIBs possess ionization energies in the range 10.0 to 13.5 eV (Sonnentrucker et al. 1997), which is consistent with larger species than studied here. In contrast, they conclude that the λ6379 Å carrier is ionized between 6−9 eV, consistent with a neutral carrier.

4. Conclusions

We have calculated excitation spectra, taking into account the FC and Duschinsky effects, for a range of closed-shell aromatic hydrocarbon cations. It is found that the theoretical procedure reproduced the long FC progression osberved by Nagy et al. for the benzylium cation. Larger cations, such as indanylium and 1-naphthylmethylium were found to have extensive FC behavior, but quenched as compared to benzylium. Fluorenylium was found to be even less FC active, especially in its $S_2 \leftarrow S_0$ transition. Since carriers of the DIBs should exhibit spectra dominated by a single vibronic transition, our results demonstrate that closed-shell cations larger than fluorenylium may present spectra with the required properties. Furthermore, the calculated ionization energies of a range of CSCs were found to be in the 13−14 eV range, consistent with variations in behavior of the DIB carriers with respect to various astrophysical environments. There are a number of experimental groups now investigating the gas-phase spectra of closed-shell aromatic hydrocarbon cations. As results flow in the coming years, we shall either witness the resolving of a 90 year old problem in astronomy, or its further confounding.

Acknowledgements. This research was supported under the Australian Research Council's Discovery funding scheme (Project Numbers DP0985767 and DP120102559). T.P.T. acknowledges the University of Sydney for a University Postgraduate Award, S.A.R. acknowledges the receipt of a Way-Klinger sabbatical fellowship from Marquette University.

References

Alata, I., Omidyan, R., Broquier, M., et al. 2010, Phys. Chem. Chem. Phys., 12, 14456
Alata, I., Broquie, M., Dedonder, C., Jouvet, C., & Marceca, E. 2012, Chem. Phys., 393, 25
Allain, T., Leach, S., & Sedlmayr, E. 1996, A&A, 305, 602
Allamandola, L. J., Tielens, A. G. G. M., & Barker, J. R. 1985, ApJ, 290, L25
Becke, A. D. 1993, J. Chem. Phys., 98, 5648
Bréchignac, P., & Pino, T. 1999, A&A, 343, L49
Cami, J., Bernard-Salas, J., Peeters, E., & Malek, S. E. 2010, Science, 329, 1180
Chalyavi, N., Troy, T. P., Nakajima, M., et al. 2010, J. Phys. Chem. A, 115, 7959
Dunning Jr., T. H. 1989, J. Chem. Phys., 90, 1007
Foing, B. H., & Ehrenfreund, P. 1994, Nature, 369, 296
Foing, B. H., & Ehrenfreund, P. 1997, A&A, 319, L59
Frisch, M. J., Trucks, G. W., Schlegel, H. B., et al. 2009, Gaussian 09, Revision A.1, Gaussian, Inc., Wallingford, CT, 2009
Garkusha, I., Fulara, J., Nagy, A., & Maier, J. P. 2011a, ApJ, 728, 131
Garkusha, I., Fulara, J., Sarre, P. J., & Maier, J. P. 2011b, J. Phys. Chem. A, 115, 10972
Geballe, T. R., Najarro, F., Figer, D. F., Schlegelmilch, B. W., & de la Fuente, D. 2011, Nature, 479, 200
Herbig, G. H. 1995, Annu. Rev. Astrophys., 33, 19
Hobbs, L. M., York, D. G., Thorburn, J. A., et al. 2009, ApJ, 705, 32
Jenniskens, P., Foing, B. H., & Ehrenfreund, P. 1994, A&A, 281, 517
Kendall, R. A., Dunning Jr., T. H., & Harrison, R. J. 1992, J. Chem. Phys., 96, 6796
Kokkin, D. L., Troy, T. P., Nakajima, M., et al. 2008, ApJ, 681, L49
Krełowski, J., Beletsky, Y., Galazutdinov, G. A., et al. 2010, ApJ, 714, L64
Krełowski, J., Galazutdinov, G., & Kołos, R. 2011, ApJ, 735, 124
Lee, C., Yang, W., & Parr, R. G. 1988, Phys. Rev. B., 37, 785
Leger, A., & D'hendecourt, L. 1985, A&A, 146, 81
Leger, A., & Puget, J. L. 1984, A&A, 137, L5
Linnartz, H., Wehres, N., Van Winckel, H., et al. 2010, A&A, 511, L3
Maier, J. P., Walker, G. A. H., & Bohlender, D. A. 2004, ApJ, 602, 286
Maier, J. P., Chakrabarty, S., Mazzotti, F. J., et al. 2011a, ApJ, 729, L20
Maier, J. P., Walker, G. A. H., Bohlender, D. A., et al. 2011b, ApJ, 726, 41
Malloci, G., Joblin, C., & Mulas, G. 2007, A&A, 462, 627
Nagy, A., Fulara, J., Garkusha, I., & Maier, J. P. 2011a, Angew. Chem. Int. Ed., 50, 3022
Nagy, A., Fulara, J., & Maier, J. P. 2011b, J. Am. Chem. Soc., 133, 19796
O'Connor, G. D., Troy, T. P., Roberts, D. A., et al. 2011, J. Am. Chem. Soc., 133, 14554
Oka, T., & McCall, B. J. 2011, Science, 331, 293
Rabrenovíc, M., Proctor, C. J., Ast, T., et al. 1983, J. Phys. Chem., 87, 3305
Reilly, N. J., Kokkin, D. L., Nakajima, M., et al. 2008, J. Am. Chem. Soc., 130, 3137
Reilly, N. J., Nakajima, M., Troy, T. P., et al. 2009, J. Am. Chem. Soc., 131, 13423
Salama, F., Bakes, E. L. O., Allamandola, L. J., & Tielens, A. G. G. M. 1996, ApJ, 458, 621
Salama, F., Galazutdinov, G. A., Krełowski, J., et al. 2011, ApJ, 728, 154
Sarre, P. J. 2006, J. Mol. Spectrosc., 238, 1
Schmidt, M. W., Baldridge, K. K., Boatz, J. A., et al. 1993, J. Comput. Chem., 14, 1347
Sebree, J. A., Kislov, V. V., Mebel, A. M., & Zwier, T. S. 2010, J. Phys. Chem. A, 114, 6255
Sebree, J. A., Kidwell, N. M., Buchanan, E. G., Zgierski, M. Z., & Zwier, T. S. 2011, Chem. Sci., 2, 1746
Snow, T. P., & Witt, A. N. 1995, Science, 270, 1445
Sonnentrucker, P., Cami, J., Ehrenfreund, P., & Foing, B. H. 1997, A&A, 327, 1215
Troy, T. P., Nakajima, M., Chalyavi, N., et al. 2009, J. Phys. Chem. A, 113, 10279
Troy, T. P., Chalyavi, N., Menon, A. S., et al. 2011, Chem. Sci., 2, 1755
Vanderzwet, G. P., & Allamandola, L. J. 1985, A&A, 146, 76
Western, C. M. 2010, PGOPHER, a Program for Simulating Rotational Structure, Version 7.1.108, University of Bristol, http://pgopher.chm.bris.ac.uk
Zhao, Y., & Truhlar, D. G. 2008, Theor. Chem. Acc., 120, 215